X-ray scattering from dislocation arrays in GaSb

2002 J. Phys.: Condens. Matter 14 13505

(http://iopscience.iop.org/0953-8984/14/49/308)

INSTITUTE OF PHYSICS PUBLISHING JOURNAL OF PHYSICS: CONDENSED MATTER

J. Phys.: Condens. Matter **14** (2002) 13505–13528 PII: S0953-8984(02)53196-9

X-ray scattering from dislocation arrays in GaSb

A Yu Babkevich[1], R A Cowley[1], N J Mason[1], S Weller[1] and A Stunault[2]

[1] Clarendon Laboratory, Oxford University, Parks Road, Oxford OX1 3PU, UK
[2] XMaS, ESRF, BP220, 38043 Grenoble Cedex, France

Received 9 September 2002
Published 29 November 2002
Online at stacks.iop.org/JPhysCM/14/13505

Abstract

The structure of GaSb layers grown epitaxially on GaAs(001) substrates has been studied by high-resolution x-ray diffraction. The samples with thicknesses between 95 and 2845 Å were grown in Oxford by metal–organic vapour phase epitaxy. The large lattice mismatch is largely relaxed by two intersecting regular arrays of 90° dislocations along the [110] and [1$\bar{1}$0] directions. The density of the dislocations changes with the thickness but the dislocations remain localized at the interface and both the GaSb layers and GaAs substrates are distorted. The spacing between the dislocations in both the [110] and [1$\bar{1}$0] directions decreases while the relaxation increases as the layer thickness increases. We have found the spacing of the dislocations, relaxation and residual in-plane strain along the [110] and [1$\bar{1}$0] directions and showed a strong asymmetry in dislocation spacing and relaxation between the two directions. This is because adjacent {110} planes in the zincblende structure are not equivalent as discussed by Abrahams and Buiocchi. Due to this asymmetry the structure of the GaSb layers is orthorhombic. Scattering from the thinner, $\lesssim$450 Å, layers shows that the GaSb grows in islands first and their size and distribution is different along the [110] and [1$\bar{1}$0] directions. The 60° dislocations in this system only appear in thick, $\gtrsim$1200 Å, layers and their density is significantly higher along the [110] direction. The results show the power of high-resolution x-ray diffraction for studying non-destructively growth, relaxation and dislocation structure of thin films and for providing detailed quantitative information about the distortions caused by misfit dislocations in epitaxial layers.

(Some figures in this article are in colour only in the electronic version)

1. Introduction

The growth of epitaxial thin layers with a low concentration of structural defects is of vital importance for the semiconductor industry because of the potential technological applications, for example, in thermophotovoltaic devices and satellite solar cells [1]. Usually there is a mismatch of the lattice parameters between the substrate and the layer so that the layer is

strained. The energy of the strain builds up with the thickness of the layer and can be relieved by dislocations if the thickness exceeds a certain critical value. The lattice mismatch between GaSb and GaAs is large, 7.8%, and so the critical thickness for the onset of dislocations will be few if any atomic layers. The structure of GaSb layers grown by molecular beam epitaxy (MBE) and by metal–organic vapour phase epitaxy (MOVPE) has been extensively studied, particularly with electron microscopy (transmission electron microscopy (TEM) or high-resolution transmission electron microscopy (HRTEM)) [2–13]. The results show that GaSb layers with an average thickness less than 50–100 Å grow three-dimensionally and consist of isolated islands [8, 13], while GaSb layers thicker than 500–800 Å form a continuous layer and the growth is then two dimensional [4, 13]. For all the layers, the GaSb is largely relaxed and the residual strain in the layers is reported to be only about 0.3–0.6% [4, 14]. HRTEM measurements have shown that the lattice parameter difference between the GaAs substrate and GaSb is relaxed by regular arrays of Lomer dislocations (90° misfit dislocations) with Burgers vectors in the plane of the GaAs/GaSb interface and aligned along the [110] and [1$\bar{1}$0] directions [3, 4, 7–11, 14]. The creation of regular arrays of Lomer dislocations is possibly directly related to the 3D growth [9]. In contrast, 60° dislocations are believed to be created when the islands coalesce [5, 8], if the islands are large and of irregular shape [11] and if the layers are grown at relatively high $>540\,^{\circ}$C) temperatures [6]. The spacing of the Lomer dislocations, D, is typically 54–58 Å [2–4, 7–11], consistent with the misfit being largely accommodated by arrays of Lomer-type misfit dislocations. If most of the strain was relieved by 60° dislocations, the average dislocation spacing would be about $D/2$, i.e. 27.5 Å.

We have used high-resolution x-ray scattering techniques to study GaSb layers grown on GaAs(001) substrates and this paper reports the results. They give a detailed quantitative picture of the evolution of the dislocation structure with the thickness. In our earlier publication [15] we reported results for two samples, with thicknesses of 130 and 3270 Å, and showed:

(i) that the crystallographic structure of the GaSb layers was orthorhombic due to the strain being relaxed by different amounts in the [110] and [1$\bar{1}$0] directions,

(ii) that the 90° dislocations are located precisely at the interface and give rise to distortions of both the GaSb layer and of the GaAs buffer layer and

(iii) that the scattering changes from being characteristic of islands to being characteristic of a mosaic crystal as the thickness increases.

It is also of interest to compare these results with those we obtained for GaSb layers on InAs substrates [16]. In this case the lattice mismatch is only 0.6% and is relaxed by networks of 60° dislocations.

As discussed in [17–20] zincblende structures grown on (001) substrates have orthogonal arrays of Lomer or 60° dislocations that reside on different sublattices. As a result of this asymmetry the misfit 60° dislocations of the same sign tend to be randomly distributed in one of the ⟨110⟩ directions and periodically distributed in the orthogonal ⟨110⟩ direction [18]. A similar asymmetry was proposed [17] for the Lomer dislocations because the two orthogonal Lomer dislocations lie on different (001) planes and may lead to a different density of misfit dislocations in the two orthogonal ⟨110⟩ directions [21]. This can give rise to different shape parameters for the Bragg peaks and different characteristic diffuse scattering along the [110] and [1$\bar{1}$0] directions in reciprocal space, as indeed observed in our x-ray experiments.

In this publication we report on measurements for ten different layer thicknesses of GaSb layers on GaAs substrates. In the next section we describe the growth of the layers and the x-ray measurements. The results are described in section 3 and then discussed in section 4.

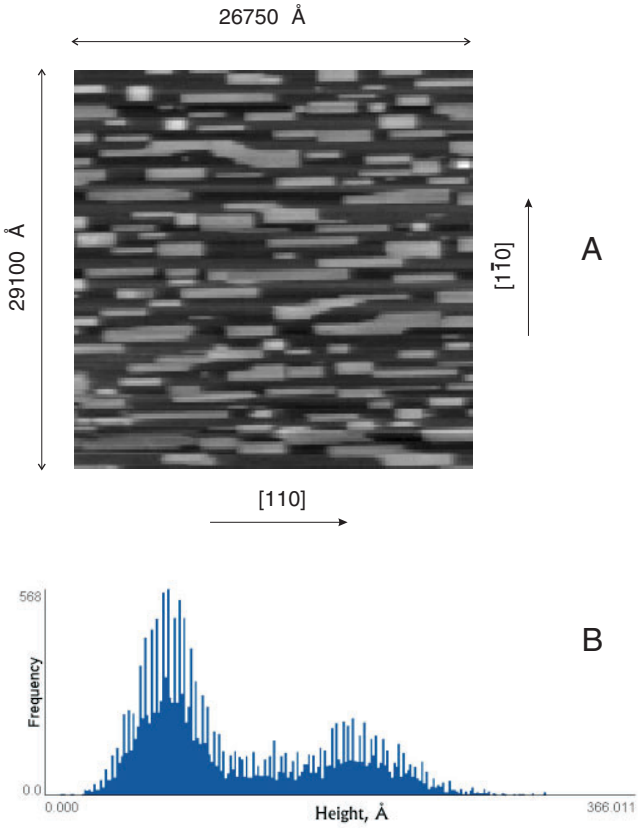

Figure 1. An AFM image of the layer with a thickness of 123 Å.

2. Experiments

The layers were grown using the MOVPE growth reactor at the Clarendon Laboratory in Oxford [22]. Si-doped (001)-oriented GaAs slices were used as substrates. The growth temperature was 520 °C and the growth rate was typically 1 μm h^{-1}. Initially a buffer layer of 1 μm of GaAs was grown on the substrate and then layers of GaSb of different thicknesses were grown by varying the growth time between 0.3 min for the thinnest sample and 42.5 min for the thickest one, as shown in table 1. For the thin samples, the GaSb layers consisted of islands as shown by the result of atomic force microscopy (AFM) measurements in figure 1. The results show that the islands are asymmetric and are more elongated along the [1$\bar{1}$0] direction than along the [110] direction.

The x-ray scattering measurements were largely performed with the XMaS beam-line (BM28) at the European Synchrotron Research Facility (ESRF). A four-circle diffractometer was used in a vertical scattering plane with the x-ray wavelength chosen to be 1.127 16 Å. The resolution of the instrument was typically 6.0×10^{-4} Å^{-1} in the scattering plane and 0.036 Å^{-1} perpendicular to the scattering plane for the (002) Bragg reflections. Preliminary measurements and measurements that did not require the high flux of a synchrotron source were performed using a laboratory triple-axis diffractometer in Oxford. The measurements were made in the $\boldsymbol{q}_x/\boldsymbol{q}_z$ scattering plane where the $\boldsymbol{q}_z$ vector was along the [001] growth direction

Table 1. Thickness of GaSb layers determined by different methods.

Sample No	Growth time (min)	Thickness (Å)						Growth rate (Å min^{-1})
		Fringes	GaSb(002) equation (2)	Gaussian equation (4)	Lorentzian equation (5)	Langford equations (6)–(8)	Final	
3346	0.33	93.4	93	98	53	105	095 ± 3	288 ± 23
3337	0.66	123.9	120	124	66	132	123 ± 2	186 ± 10
3032	0.75	155.3	169	176	100	188	167 ± 11	223 ± 18
3336	1.35	233.2	211	217	122	231	220 ± 11	163 ± 11
3335	2.40	313.7	293	301	164	304	303 ± 10	131 ± 5
3192	4.00	—	602	659	396	586	660 ± 30	126 ± 6
3338	9.70	—	936	1111	749	958	1110 ± 90	114 ± 9
3333	21.00	—	1268	1588	1260	1685	1590 ± 160	76 ± 8
3329	32.00	—	1692	2220	2133	1834	2220 ± 260	69 ± 8
3426	42.50	—	2329	2844	2876	3049	2845 ± 260	67 ± 6

and $\boldsymbol{q}_x$ was either along the [110] or [1$\bar{1}$0] direction in reciprocal space. In this system of coordinates the positions of the Bragg peaks are given in terms of two wavevector transfer components $q_x = |\boldsymbol{q}_x| = \frac{2\pi}{d_{\langle 110\rangle}}$ and $q_z = |\boldsymbol{q}_z| = \frac{2\pi}{d_{001}}$. For convenience, Bragg reflections will usually be denoted by conventional triple Miller indices HKL rather than by their (q_x, q_z) coordinates. Scans varying the wavevector transfer through a Bragg reflection along $\boldsymbol{q}_z$ are called longitudinal scans and those varying it along $\boldsymbol{q}_x$ are called transverse scans.

3. Experimental results

3.1. Thickness of the layers

The thickness of a single layer deposited on a substrate should be readily measured by x-ray diffraction. If the roughness of the surface is sufficiently small, the thickness can be found from the separation between the Kiessig fringes in the x-ray reflectivity [23] or from longitudinal scans along the growth direction by measuring the period of the Pendellösung fringes around the Bragg reflections. This method is the most reliable, accurate and simple to use for single crystal layers but, unfortunately, the fringes can only be distinguished for relatively thin (up to about 400 Å) layers of GaSb, see table 1.

Another way of calculating the thickness is to assume that the shape of the Bragg peaks in longitudinal scans is determined by the single-slit interference function of a single layer and any contribution to the width from imperfections such as inhomogeneous strain is either negligible or sufficiently small to be ignored. The intensity of x-ray scattering at Bragg peak positions from an ideal layer with a perfectly flat surface is given by

$$I \backsim \frac{\sin^2(Nq_z d/2)}{\sin^2(q_z d/2)} \tag{1}$$

where N is a number of planes with an interplanar spacing d. The intensity at the maxima is proportional to N^2 and the relation between the thickness of the film $T = Nd$ and the full width at half maximum (FWHM) w_z of the Bragg peak given by equation (1) is

$$T = \frac{5.566\,24}{w_z}. \tag{2}$$

This analysis assumes that the spacing of the atomic planes is uniform. If there is a non-uniform strain then the width of the Bragg peaks increases with increasing q_z or L, and the thickness

of the layer is given in principle by extrapolating the Bragg peak width to $q_z = L = 0$. The difficulty lies in making this extrapolation.

For the thinner films, the increase in the width due to strain and the instrumental resolution is only a small fraction of the total width of the Bragg reflections. The width of the GaSb(002) reflections when put into equation (2) then gives a good estimate of the layer thicknesses as shown in table 1 because these estimates of the thicknesses are in good agreement with those from the Pendellösung fringes. For the thicker samples the extrapolated width for $q_z = 0$ Å^{-1} is appreciably smaller than that for the (002) peak and so the (002) peak provides only a lower limit to the thickness of the layer. For thicker samples, subtraction of the instrumental broadening is vital for a proper extrapolation. The instrumental resolution function, IRF, was obtained from the Gaussian Bragg reflections of the substrate and changes with q_z approximately as $w_z^{IR} = 3.0467 \times 10^{-4} q_z$. For the (006) Bragg peak of GaSb, broadening due to IRF is therefore equivalent to the width of the peaks from a 3000 Å layer and for the thicker films this broadening becomes a major contribution to the width of the scattering. Considering that the GaSb Bragg peaks are essentially Gaussian, the broadening due to the instrumental resolution can be obtained from the total width as

$$(w_z^L)^2 = w_z^2 - (w_z^{IR})^2 \tag{3}$$

where the FWHM of the Bragg peaks of epitaxial layers w_z^L includes contributions from the finite thickness of the layer w_z^T and the broadening from the inhomogeneous strain w_z^s and sample defects if any. We have used the w_z^L widths extrapolated as described below to calculate the thicknesses from equation (2) and compare the results of different methods in table 1.

One way of estimating the thicknesses of the layers from the w_z^L measured at different Bragg reflections, L, is to extrapolate to $L = 0$ by assuming that the line-shape is either a pure Gaussian or Lorentzian. If the thickness and strain components are both Gaussian, the thickness can be obtained by extrapolating the $(w_z^L)^2$ versus q_z^2 plots to $q_z = 0$ so as to give w_z^T. If both thickness and strain components have a Lorentzian line-shape, then the w_z^L values are plotted versus q_z and extrapolated to $q_z = 0$ Å^{-1} as shown in figure 2. The Fourier transform of a Gaussian peak measured in reciprocal space then gives the thickness T as

$$T = -\frac{8 \ln 0.5}{w_z^T} \simeq \frac{5.545\,18}{w_z^T} \tag{4}$$

whereas a Lorentzian line-shape corresponds to a peak in direct space with a FWHM of

$$T = -\frac{4 \ln 0.5}{w_z^T} \simeq \frac{2.772\,59}{w_z^T}. \tag{5}$$

Note that coefficients in the numerator of equations (4) and (5) are different from the 2π that are often used to determine the thickness. The thicknesses obtained from equations (4) and (5) are listed in table 1 and the results suggest that equation (5) tends to underestimate the thicknesses.

We also used the method proposed by Langford for powders [24, 25]. In the case of mixed Gaussian and Lorentzian line-shapes the components are separated by fitting them with a Voigt function to get β_L and β_G, which are the integral breadths $(=\frac{\text{area under the peak}}{\text{peak intensity}})$ of the Gaussian and Lorentzian components. Extrapolating the plots of $\beta_L(q_z)$ and $\beta_G^2(q_z^2)$ to $q_z = 0$ the two widths β_L^0 and β_G^0 are found. The total integral breadth β at $q_z = 0$ corresponding to a q-independent component of peak broadening is obtained by Langford [25] as

$$\beta = \frac{\beta_G^0}{\exp(y^2)(1 - \operatorname{erf}(y))} \tag{6}$$

where

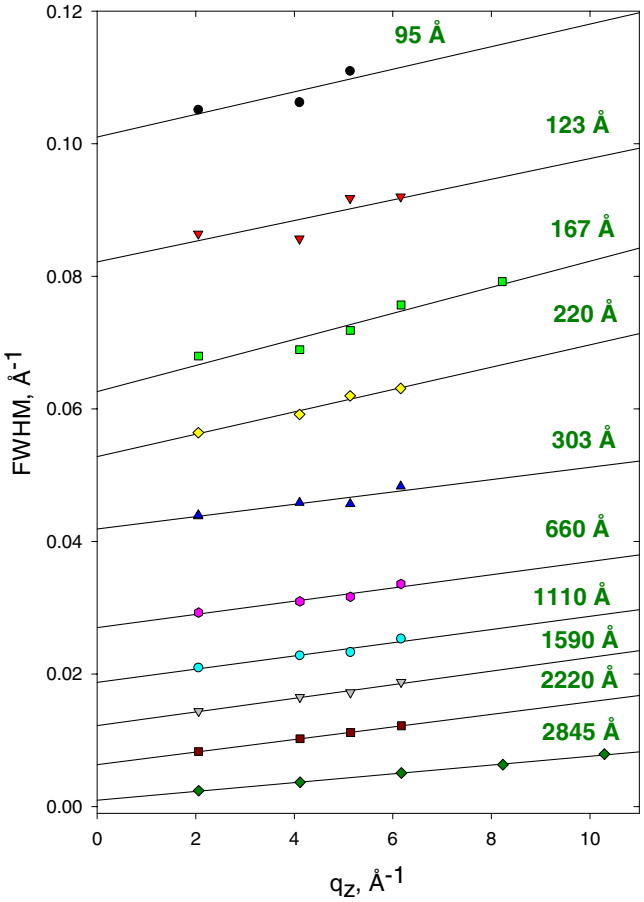

Figure 2. FWHM of the GaSb Bragg peaks in the [00L] direction. The data are shifted vertically by 0.005 Å^{-1} for clarity.

$$y = \frac{\beta_L^0}{\sqrt{\pi}\beta_G^0}. \tag{7}$$

The thicknesses of the films T are then given by

$$T = \frac{2\pi}{\beta}. \tag{8}$$

The results of using this procedure are given in table 1 and show reasonable agreement with the values obtained by other methods. In table 1 we summarize the results obtained by these different methods and present our best estimates of the thicknesses of the layers. We assumed that for thinner layers the Pendellösung fringes and equations (2) and (4) provide the most accurate estimate of the thickness and for thicker films the most accurate values are obtained from equation (4). Langford's method, which obtains the thicknesses in a different way, equations (6)–(8), gives reasonable agreement with our best estimates of the thicknesses.

The growth rate of the layers is shown in table 1 and demonstrates that the growth slows down after the first few minutes. This decrease in the growth rate is possibly explained in part because when the layers are thin the measured height of the islands is larger than the average thickness because the x-rays do not average over the areas between the islands. It is

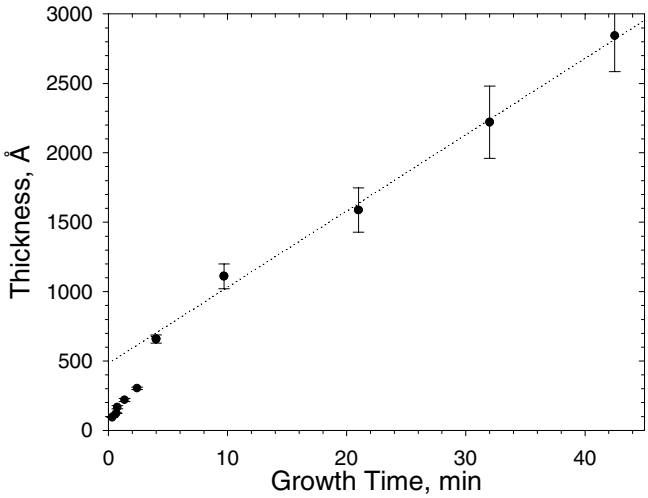

Figure 3. Variation of the thickness of the GaSb layers with growth time.

more likely, however, to be because the coalescence of the islands leaves a slow-growing (001) surface after annihilation of fast-growing (111) facets when the growth changes from a 3D to 2D mode. The variation of the thickness with the growth time is presented in figure 3 and shows an almost linear increase of the thickness with a growth time, t, so that after the first 4 min of growth $T \cong 485 + 55t$ Å.

An alternative approach for obtaining the thickness is to measure the absolute intensity of the Bragg reflections and if the kinematical theory is adequate, as used above, the intensity is proportional to the thickness. It is, however, difficult to obtain the integrated intensity accurately because the experimental conditions needed conflict with those required for high resolution and the theory assumes that the structure and constituents of the layer are well known. We have not attempted to use this way of determining the thickness.

Besides describing the determination of the thicknesses of our samples, this section shows that it can be unexpectedly difficult to determine the thickness of thin films using x-ray diffraction techniques. It is not reliable to determine the thickness from the width of the Bragg reflection and using equation (1), as is frequently done in the literature. The layers are frequently inhomogeneously strained when it is necessary to measure the width of several Bragg reflections and then to see if they all give the same thickness. It they do, then equation (2) gives an accurate answer but if not then it is necessary to extrapolate the width to zero wavevector transfer to obtain the thickness.

3.2. Uniform and non-uniform strain

The lattice parameters of bulk GaSb and GaAs are $a_L = 6.0954$ Å, $a_S = 5.653\,15$ Å respectively. The lattice mismatch, defined as

$$f_m = \frac{a_L - a_S}{a_S}, \tag{9}$$

is large, 7.82%, and therefore the development of large strains when a GaSb layer is grown on the GaAs substrate is inevitable. As the thickness, T, increases there is a build-up of elastic energy in the film and the mechanism to release this energy is the creation of misfit dislocations which begin to set in once the thickness reaches the critical thickness, T_c. Due to the large lattice

Table 2. 90° dislocation spacing and the corresponding relaxation of the GaSb layers.

Sample No	T, (Å)	δ (Å)		D (Å)		$a_l^{\parallel}$ (Å)		R (%)		$\varepsilon_{res}^{\parallel}$ (%)	
		[110]	[1$\bar{1}$0]	[110]	[1$\bar{1}$0]	[110]	[1$\bar{1}$0]	[110]	[1$\bar{1}$0]	[110]	[1$\bar{1}$0]
3346	95	0.101 43(9)	—	61.94(5)	—	6.0431(4)	—	88.18(8)	—	−0.858	—
3337	123	0.102 39(16)	0.110 48(21)	61.37(10)	56.87(11)	6.0471(7)	6.0806(9)	89.07(15)	96.64(20)	−0.793	−0.244
3336	220	0.102 72(7)	—	61.17(4)	—	6.0484(3)	—	89.38(7)	—	−0.771	—
3335	303	—	0.111 48(22)	—	56.36(11)	—	6.0847(9)	—	97.58(21)	—	−0.176
3192	660	0.105 89(57)	0.112 03(11)	59.34(32)	56.09(5)	6.0615(24)	6.0870(4)	92.33(53)	98.10(10)	−0.556	−0.138
3338	1110	0.105 74(44)	0.111 97(14)	59.42(25)	56.11(7)	6.0609(18)	6.0867(6)	92.19(41)	98.04(13)	−0.566	−0.142
3333	1590	0.108 55(62)	0.112 73(46)	57.88(33)	55.74(23)	6.0725(26)	6.0899(19)	94.83(58)	98.76(43)	−0.375	−0.090
3329	2220	0.109 20(44)	0.112 93(8)	57.54(23)	55.64(4)	6.0752(18)	6.0908(3)	95.43(42)	98.95(7)	−0.331	−0.076

mismatch, the critical thickness in GaSb/GaAs is small and, as we shall show in the next section, the strain in GaSb layers is indeed largely relaxed by regular arrays of 90° dislocations located at the interface between the GaSb and the GaAs substrate (or more precisely between the layer and the GaAs buffer layer). The samples we have measured are an order of magnitude or more thicker than the critical thickness for the 90° dislocations and dislocation arrays were observed in all layers. Therefore the remaining or residual strain defined as $\varepsilon_{res}^{\parallel} = (a_l^{\parallel} - a_L)/a_L$, where $a_l^{\parallel}$ is the in-plane lattice constant of the layer, is relatively small compared to what it would be if the whole lattice mismatch of the bulk materials was producing strain (see table 2).

The relaxation of the strain in the two perpendicular directions, [110] and [1$\overline{1}$0], is different as demonstrated by the data in table 2 and figure 4. Figure 4 shows the variation with the thickness of the $\Delta q_z = q_s^{\perp} - q_l^{\perp}$ and $\Delta q_x = q_s^{\parallel} - q_l^{\parallel}$ where $q_s^{\parallel}$ and $q_l^{\parallel}$ are the positions of the off-axis (115) reflections from the substrate and from the film measured in transverse scans along one of the $\langle 110 \rangle$ directions and $q_s^{\perp}$ and $q_l^{\perp}$ are the positions of the substrate and layer on-axis peaks measured in longitudinal scans through the $(00L)$ Bragg reflections. Figure 4(b) shows that in the plane of the film the relaxation is significantly smaller along the [110] direction than in the perpendicular [1$\overline{1}$0] direction, i.e. there is an anisotropy in the relaxation. If the relaxation is described by the relaxation parameter $R = \Delta q_x/(q_S - q_L)$ where q_S and q_L are the positions of the off-axis reflections from the substrate and from bulk material of the layer then, for the thin 123 Å layer the relaxation is 89.07% in the [110] direction and 96.64% in the [1$\overline{1}$0] direction. As the thickness increases, the relaxation increases and for the thickest films the relaxation is almost complete in both directions, see figure 4(b) and table 2. The Δq_x values shown in figure 4(b) and elasticity theory were used to calculate the strain in the growth direction and the results for Δq_z are shown in figure 4(a) (dashed line). The calculations are smaller than the observed values by an approximately constant amount of 0.0025 Å^{-1}.

As the thickness of the film increases, there is a possibility that the strain will be further relieved by a network of 60° dislocations. There may then be a random strain and also a uniform strain gradient throughout the layer. We shall now consider the implications of these strains on the x-ray scattering.

In our earlier publication [16] we showed that a linear lattice parameter variation between the top and bottom of the layer gave rise to a contribution to the width of the Bragg reflections that increased proportionally to q_z. In contrast, a series of random strains with a Gaussian distribution gave a contribution that increased as q_z^2. We have therefore studied the wavevector dependence of the Bragg peak widths and the results are shown in figure 2. The FWHM of the Bragg peaks increases approximately linearly with the wavevector q_z and the slope of the lines is larger for the thinner, 95–220 Å thick, layers compared to the thicker, 303–2845 Å, layers. Surprisingly, the slope is approximately constant for each set of layers. Assuming that there is a linear variation of the lattice parameter between the top and bottom of the layer as before [16], we find that the change in the strain through the layer is $\gamma N = 2.0 \times 10^{-3}$ for the thin layers ($T \lesssim 260$ Å) and $\gamma N = 1.1 \times 10^{-3}$ for ($T \gtrsim 260$ Å). These changes in the strain can be compared with the difference between the lattice parameter of the layer and that of the bulk which, from figure 4, is about 3.4×10^{-3} for the thin layers and 2.2×10^{-3} for the thicker layers. The approximate agreement with the values deduced from the widths of the Bragg peaks shows that the variation in the widths shown in figure 2 does result from inhomogeneous strains. The approximately constant slope above and below ~260 Å indicates that despite an increase of the thickness of the layers the strain gradient between the top and bottom of the layers remains almost unchanged in each regime even though the change in amplitude suggests a change in the growth mechanism.

We have also observed a change in the shape of the Bragg reflections with the film thickness as shown in figure 5. The measured intensities were fitted to a Voigt function which is a

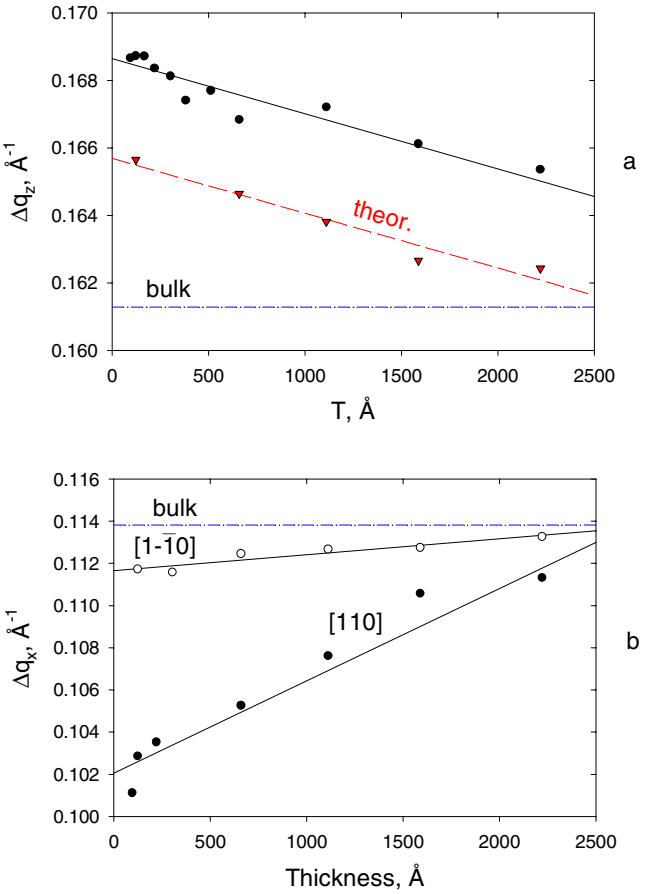

Figure 4. Spacing between the GaSb and GaAs out-of-plane (002) reflections (a) and between the in-plane components of the (115) reflections (b). Dashed line in (a) shows a spacing between the (002) Bragg peaks of the film and the substrate calculated from the elasticity theory and data in (b).

convolution of a Gaussian and a Lorentzian and in figure 5(a) we show the resulting widths of each component for the (004) reflection of GaSb. The width of the Gaussian component is the largest and decreases with increasing layer thickness. The Lorentzian component has a negligible width for the layers up to 300 Å thickness but for the thicker (>600 Å) layers the width is comparable to that of the Gaussian component. Hence there is a change in the line-shape, growth rate (figure 3) and other properties for layers with a thickness of more than 450 Å probably due to coalescence of the islands.

3.3. Misfit dislocations

The x-ray scattering observed when the wavevector transfer q is varied transversely to the (004) Bragg reflection is shown in figure 6. There is a strong peak in the scattering centred on $q_x = 0$ Å^{-1} and the detailed nature of this scattering is discussed in section 4. In this section we discuss the peaks with $q_x \approx \pm 0.11 \times n$ (where n is an integer) that are the reflections arising from the regular arrays of 90° dislocations.

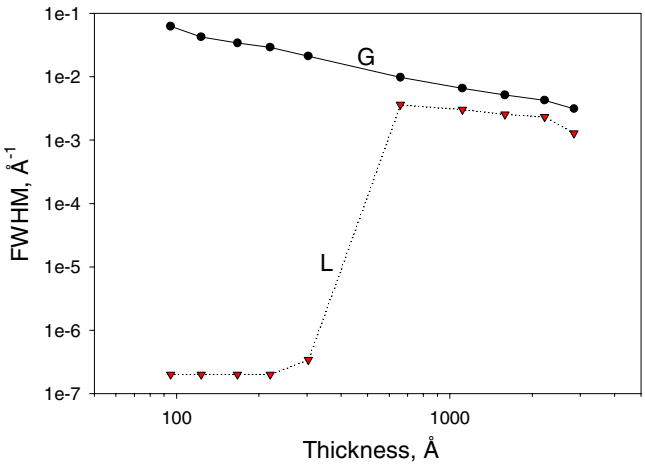

Figure 5. Gaussian (G) and Lorentzian (L) widths of fits to the GaSb(004) peaks as a function of film thickness.

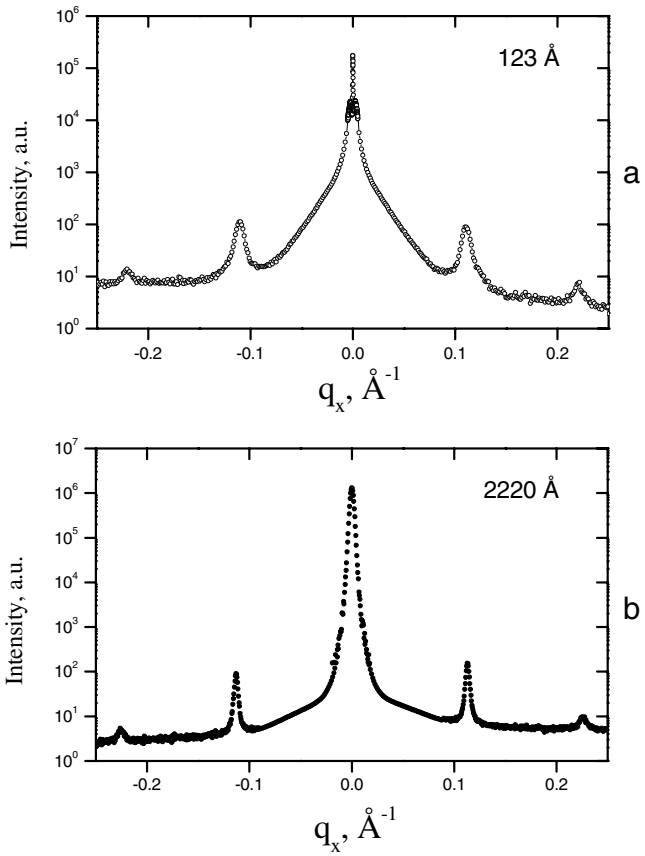

Figure 6. X-ray scattering intensity near the (004) reflection of 123 Å (a) and 2220 Å (b) layers of GaSb measured in transverse scans when the wavevector transfer is varied along the $[1\bar{1}0]$ direction.

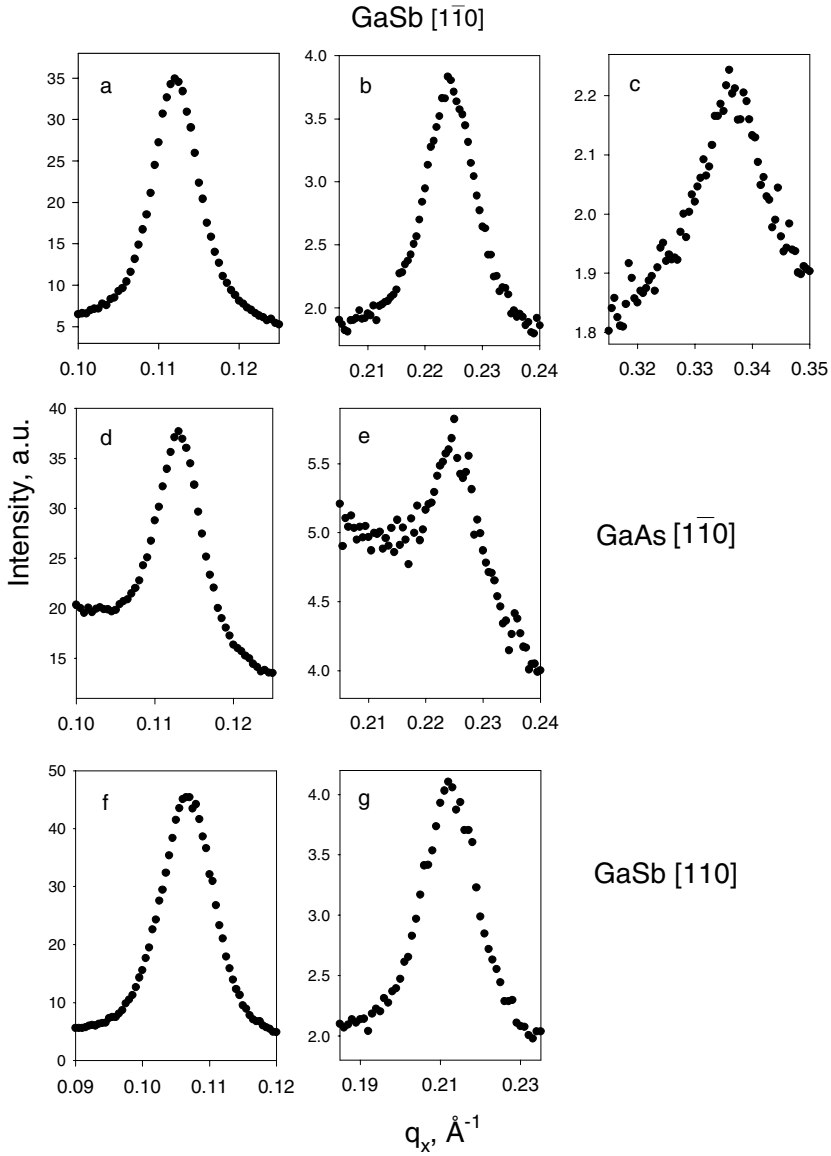

Figure 7. Satellite reflections from a regular array of 90° misfit dislocations in a 660 Å GaSb film and the GaAs buffer layer. Note different peak positions of the satellites measured along the [110] and [1$\bar{1}$0] directions.

The scattered intensity of these peaks for the 660 Å thick layer of GaSb is shown in figure 7. The results were obtained by keeping the wavevector component q_z equal to the q_z coordinate of the (004) Bragg reflection of the GaSb ($q_z = 4.111\,33$ Å^{-1}) and varying the q_x component either along the [110] or [1$\bar{1}$0] direction. The peaks in figure 7 arise from scattering by a regular array of 90° misfit dislocations that cause distortions in both the GaAs and GaSb and propagate along the [110] and [1$\bar{1}$0] directions in (001) planes parallel to the interface. The results (figures 7(a)–(c)) show three orders of satellites separated from the main GaSb Bragg peak by a distance $q_x = \delta = \pm n \times 0.112\,03(11)$ Å^{-1} when q_x is varied along

the $[1\bar{1}0]$ direction. When q_x is varied along the [110] direction as in figures 7(f), (g) the satellite peaks are centred at $q_x = \pm n \times 0.1059(6)$ Å^{-1}. There are a similar regular series of satellite peaks if q_z is set to the position of the GaAs(004) Bragg reflection (figures 7(d), (e)). The spacings between these satellite peaks are the same as those of the ones near the GaSb reflections, showing that lattice distortions on both sides of the interface are similar.

We have measured the satellites around the (002), (004) and (006) reflections of GaSb for all of the samples. Figure 8 shows that as the thickness of the GaSb layer increases, the satellite spacing δ increases in both the [110] and $[1\bar{1}0]$ directions and is systematically larger in the $[1\bar{1}0]$ direction. From the position of satellites measured for both sides of the Bragg peaks, $\pm\delta \cdot n$, the average spacing δ along the [110] and $[1\bar{1}0]$ directions has been determined for different samples and the results are presented in table 2. The spacing between the dislocations $D = 2\pi/\delta$ is also listed in table 2. If the whole of the misfit strain was relieved by 90° misfit dislocations, the spacing of the dislocations, $D = |\boldsymbol{b}|/f_m$, would be 55.095 Å. The results show that the dislocation spacing is always bigger than this and, furthermore, is anisotropic and responsible for the anisotropy of the relaxation which makes the crystal structure of the GaSb layer orthorhombic [15]. The density of dislocations is higher in the $[1\bar{1}0]$ direction and therefore the relaxation is more complete in this direction than in the [110] direction, as illustrated by figure 4 and table 2.

In figures 9(a) and (b) the wavevector of the dislocation lattice δ is compared with the difference in the position of Bragg reflections in the in-plane direction Δq_x shown in figure 4(b). The relaxation of the layer arises solely from the 90° dislocations if the values of δ and Δq_x are the same while other relaxation processes are present if they differ. The results show that for the $[1\bar{1}0]$ direction, figure 9(a), the values of δ are possibly slightly smaller than Δq_x but the difference between them is comparable to the error in Δq_x for all the layers. In contrast for the [110] direction, figure 9(b), for the thin ($\lesssim$770 Å) layers there is no significant difference between δ and Δq_x but for the thicker layers the difference is about 0.0020(5) Å^{-1}. This difference suggests that not all of the strain is relieved by the 90° dislocations but that a small part of the strain, about 1.5% of the total strain, is relieved by another mechanism. We shall suggest in section 4 that this extra strain is relieved by 60° dislocations.

Further information about the misfit dislocations was obtained from scans of the wavevector transfer along the q_z direction while the q_x component was fixed at the centre of the first-order satellite reflection of GaSb so that the scan passes through the satellite peak. A typical result is shown in figure 10 for the 660 Å thick sample. There are two peaks which have q_z components corresponding to the GaSb and GaAs(004) Bragg reflections respectively. The intensities of both peaks in figure 10(b) are comparable and the widths of the peaks are 0.178(1) Å^{-1} for the GaSb peak and 0.199(1) Å^{-1} for the GaAs peak. These widths change only slightly when the thickness of the layer increases and the average of all the measured FWHMs are 0.176(3) and 0.198(3) Å^{-1} correspondingly. These results demonstrate that both the GaAs substrate and GaSb layer are distorted by the dislocations and that their distortions extend about 32–36 Å into both materials. Since these distortions and peak intensities are similar for both materials, the dislocations must be located at the interface between the GaSb and the GaAs. This conclusion disagrees with that of Mallard *et al* [10], who suggest that the initial stages of GaSb deposition produce a commensurate, defect-free layer of approximately three or four monolayers (<15 Å) before the lattice relaxation starts to occur by the nucleation of misfit dislocations at the epilayer surface, resulting in the creation of a number of islands of elastically relaxed GaSb. Our data show no evidence for such a layer and suggest that the misfit dislocations occur at the interface between the GaAs and GaSb.

The widths of the satellite peaks increase with the peak index as shown in figure 11. The average ratio of the FWHM of the second-order ($n = 2$) satellites to the FWHM of the first-

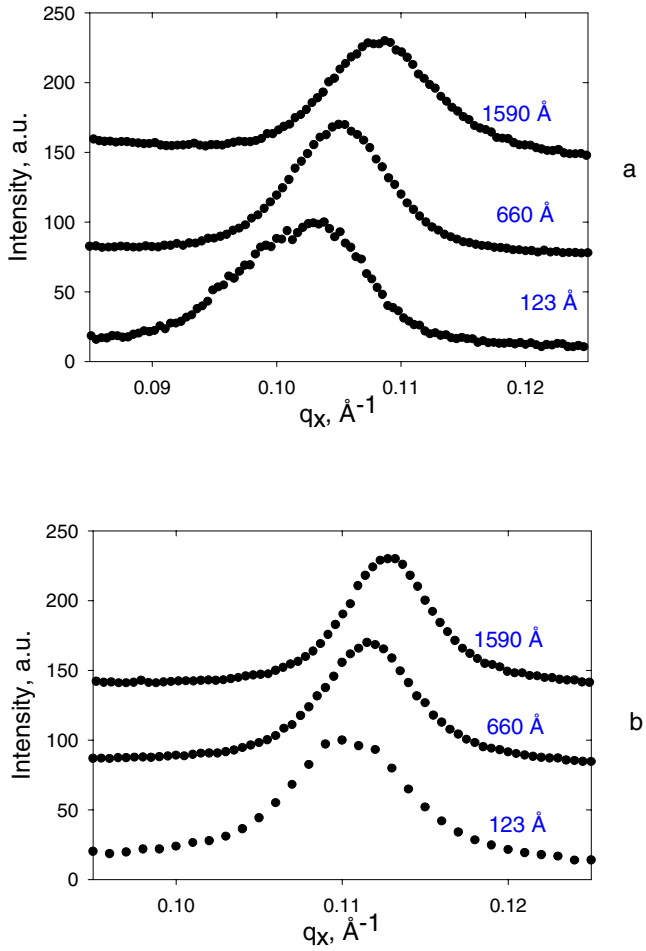

Figure 8. Variation of the position of satellites around the GaSb(004) Bragg peaks with the layer thickness measured in scans along the [110] (a) and [1$\bar{1}$0] (b) directions.

order ($n = 1$) satellites is 1.8(3) for the satellites in the [110] direction, figure 11(a). For the satellites in the [1$\bar{1}$0] direction around the (004) peaks the FWHM increases from the first-to the second-and third-order ($n = 3$) satellites as 1:1.4(1):2.1(2). This increase in the width shows that there is a cumulative disorder in the spacing of the dislocations, that is any variation of the spacing alters the positions of all subsequent dislocations in the dislocation array. The width of the first-order satellites measured around the (002) and (004) Bragg reflections was larger in the [110] direction than for the [1$\bar{1}$0] direction, figure 11(b), suggesting that the dislocation array is less ordered along the [110] direction. An average width of the first-order satellites around the (002) Bragg reflections gives a correlation length for the dislocation array of 786(140) Å in the [110] direction and for the [1$\bar{1}$0] direction the correlation length is 1396(200) Å.

3.4. Islands and 60° misfit dislocations

The x-ray scattering centred on $q_x = 0$ was measured around the Bragg reflections of GaSb in transverse scans by varying the wavevector transfer along the [110] and [1$\bar{1}$0] directions, as shown in figures 12–15. The scattering changes dramatically as the thickness of the samples

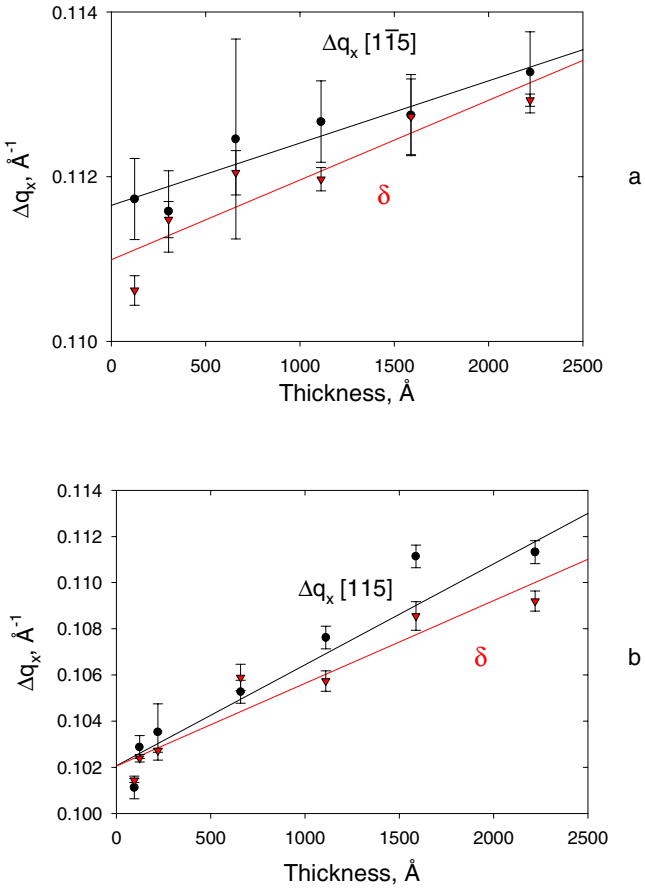

Figure 9. The difference between the in-plane wavevectors of the GaSb and GaAs(115) peaks (filled circles) and the difference between the (002) Bragg reflections and the position of satellite peaks (δ) from regular 90° dislocation arrays: (a) is for measurements with the wavevector transfer parallel to the $[1\bar{1}0]$ direction, (b) is for measurements with the wavevector transfer parallel to the [110] direction.

increases, figures 12 and 13. For convenience the features of the x-ray scattering from thin and thick layers will be considered separately and for the purpose of this analysis we assume that the transition between the two regimes occurs at about 600 ± 200 Å.

3.4.1. Thin layers. The scattering observed from the thin layers is illustrated in figures 13(b) and 14 for the layer with a thickness of 123 Å. The results are typical of the scattering from all the thin layers. When the wavevector transfer is varied along either the [110] or $[1\bar{1}0]$ direction close to the Bragg reflection of the GaSb, the scattering consists of a Bragg component that is narrow in wavevector transfer and a broader diffuse component centred at or close to the position of the Bragg component. The fraction of the intensity in the Bragg component decreases when either the index L of the $(00L)$ Bragg reflection or the layer thickness is increased. In more detail, the experimental results for the layer with a thickness of 123 Å show Bragg peaks with widths of 0.000 40(3) Å^{-1} for (002), which increases proportional to q_z for the (004) and (006) Bragg reflections. The fraction of the total intensity in the Bragg peaks component reduces from about 30% at (002) to about 7% at (006).

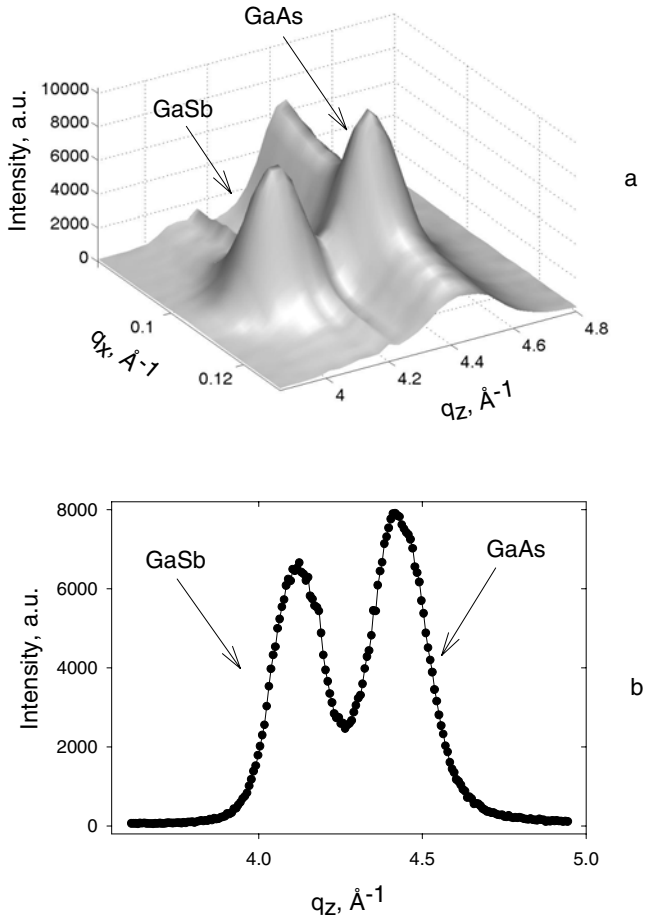

Figure 10. Reciprocal space map around the first order satellite reflections of (004) GaSb and GaAs (a), and a longitudinal scan through both satellites for $q_x = 0.106\,76$ Å^{-1} (b).

The diffuse component of the data when the wavevector transfer was scanned along the [110] direction could be effectively described as a single peak with broad Lorentzian-like wings. The width increased with increasing L value of the Bragg reflection. For example, for the sample with a thickness of 220 Å the widths are 0.003 49(11), 0.004 38(20) and 0.005 79(35) Å^{-1} near the (002), (004) and (006) reflections respectively. The behaviour is neither independent of L nor proportional to L suggesting that there is not a simple explanation of this behaviour as we shall discuss further in section 4.

When the wavevector transfer was varied along the [1$\bar{1}$0] direction the results for the broad component were more complicated. Figure 13(b) shows the measurements for the sample with a thickness of 123 Å. The broad component of the scattering near the (002) Bragg reflection consists of two broad Lorentzian peaks centred on $q_x = \pm 0.0027(1)$ Å^{-1} and having widths of 0.0040(2) Å^{-1}. Similar peaks are observed near the (004) and (006) Bragg reflections and their widths increase to 0.0053(3) and 0.0067(5) Å^{-1} respectively. The positions of the peaks are independent of L even though the widths are increasing with L but more slowly than a linear dependence.

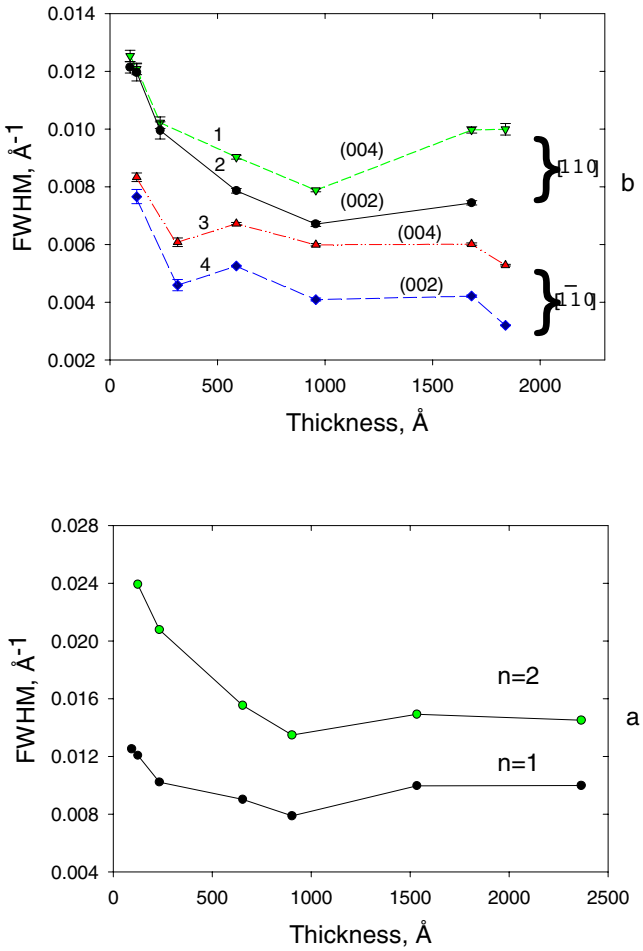

Figure 11. Variation with the thickness of the FWHM of the first-($n = 1$) and second-($n = 2$) order satellite peaks near the GaSb(004) reflection measured along the [110] direction (a) and FWHM of the first-order satellite peaks measured around the GaSb(002) and (004) reflections along the [110] and [1$\bar{1}$0] directions.

The results are more complex for the layer with a thickness of 303 Å as shown in figure 13. There is a sharp peak at $q_x = 0$ Å^{-1}. The diffuse peaks close to $q_x = 0$ Å^{-1} are less well resolved but fits to the data show that the main peak is best described by two Lorentzian peaks with $q_x = \pm 0.0018(3)$ Å^{-1} and widths of 0.0039(8) Å^{-1}. Fits to the data near the (004) and (006) Bragg reflections could not resolve the separate peaks and the data was well described by single peaks. The new feature of the data is the additional much weaker peak with $q_x = \pm 0.0273(1)$ Å^{-1} and a width of 0.0130(4) Å^{-1} near the (004) Bragg reflection.

3.4.2. Thick layers. As the thickness increases above 600 Å the scattering undergoes a steady evolution to a single peak and gradually changes to that typical of the thicker layers. This regime is characterized by the disappearance of the Pendellösung fringes in longitudinal scans and by the different components of the scattering in the transverse scans becoming indistinguishable so that the scattering can be described by a single broad component. Figure 16 shows the width

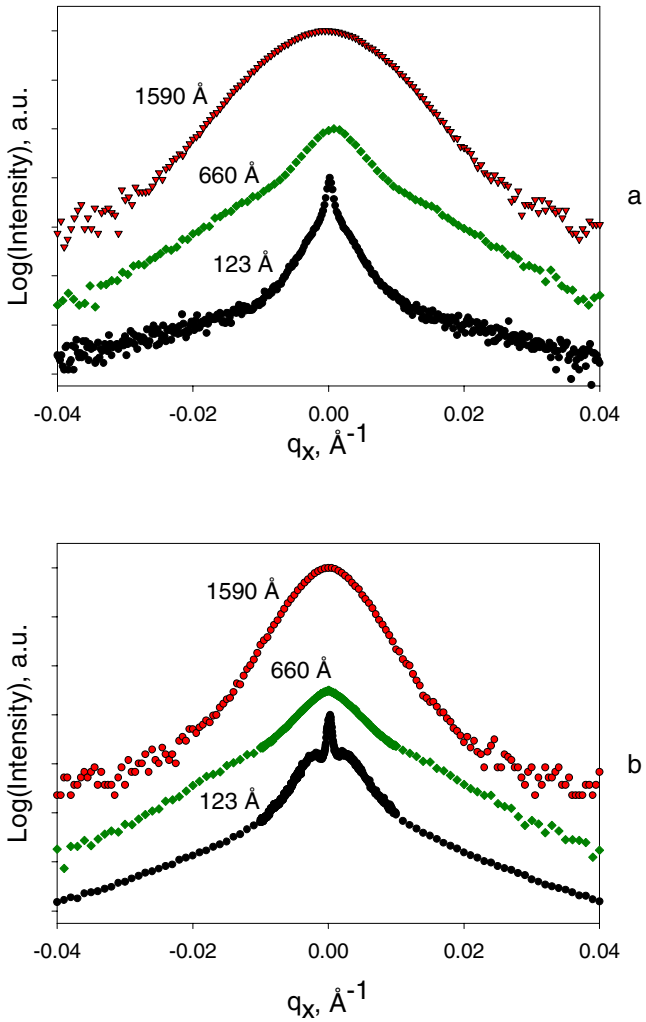

Figure 12. The intensity observed in transverse scans through the (004) Bragg peak for different thicknesses of the GaSb layer measured in a scattering plane that includes the [110] direction (a) and the [1$\bar{1}$0] direction (b).

of the broad peak near the (004) Bragg reflection as a function of thickness and orientation of the scattering plane. Along the [1$\bar{1}$0] direction the FWHM of the broad peak is largely independent of the thickness. Figure 16 also shows that there is little difference between the widths of the broad peaks measured along the [110] and [1$\bar{1}$0] directions for samples which are less than 600 Å thick. For larger thicknesses the width of the scattering increases steadily with the thickness.

When the thickness of the GaSb is larger than 1000 Å the diffraction patterns for both the [110] and [1$\bar{1}$0] directions are well described by single peaks, figure 12, with larger peak widths for the scans of the wavevector transfer along the [110] direction. The scattering from the layer with a thickness of 1590 Å has an approximately Gaussian shape and the width is 0.0070(4) Å^{-1} for (002), 0.0138(4) Å^{-1} for (004) and 0.0204(10) Å^{-1} for (006) Bragg reflections when the wavevector transfer is varied along the [110] direction and 0.0045(4) Å^{-1} for (002), 0.0079(5) Å^{-1} for (004) and 0.0112(10) Å^{-1} for (006) along the [1$\bar{1}$0] direction.

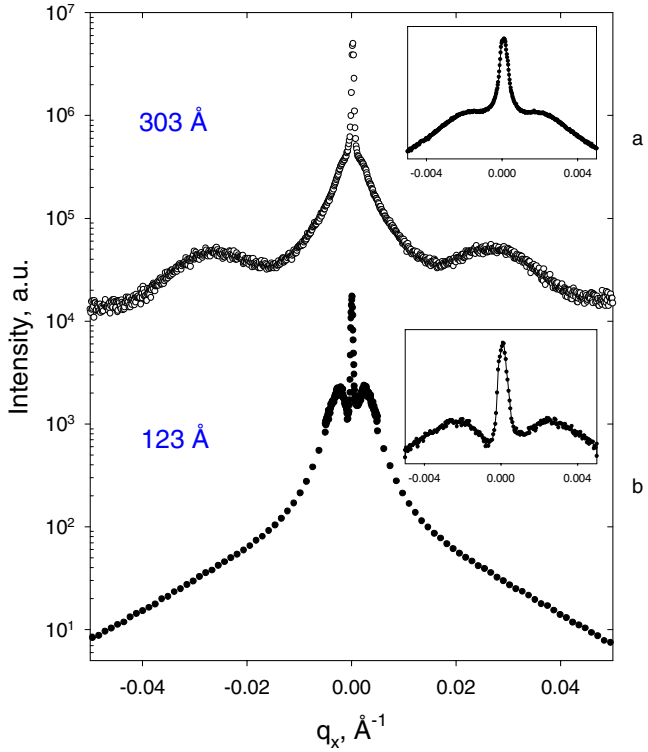

Figure 13. The intensity observed in transverse scans parallel to the [1$\bar{1}$0] direction through the (002) peak of 303 Å (a) and 123 Å (b) thick GaSb layers.

Since the widths are increasing in proportion to the wavevector transfer q_z this scattering is characteristic of the scattering from a mosaic crystal with a mosaic spread of 0.11° in the [1$\bar{1}$0] direction and 0.19° in the [110] direction. This is characteristic of a network of dislocations as described by Kaganer *et al* [26]. This theory well described the scattering from GaSb/InAs epilayers thicker than the critical thickness of about 1250 Å as we have discussed before [16]. The theory [26] for a high density of 60° misfit dislocations gives the dislocation density in terms of the width of the scattering as $\rho = (\frac{w_x^L}{21.3})^2 T$ where w_x^L is the transverse width of the scattering at the (004) Bragg reflection. Our estimates of the densities of 60° dislocations and the mean dislocation spacings are given in table 3. Both figures have errors of about 20%. The results show that the dislocation spacing decreases with increasing thickness and is smaller in the [110] direction. The 60° dislocations cause an in-plane strain for the three thickest samples of on average 0.0024 in the [110] direction and of 0.0006 in the [1$\bar{1}$0] direction and these correspond to differences between the Δq_x and δ in figure 9 for these layers of 0.0035 and 0.0009 Å^{-1}. These are somewhat larger than the differences shown in figure 9 but are of a comparable size. We conclude that the lattice parameters of the thick samples are partly relaxed by 60° dislocations.

4. Discussion

In the previous sections we have shown that x-ray scattering measurements provide detailed information about the structures of thin layers and how they change as the thickness of the

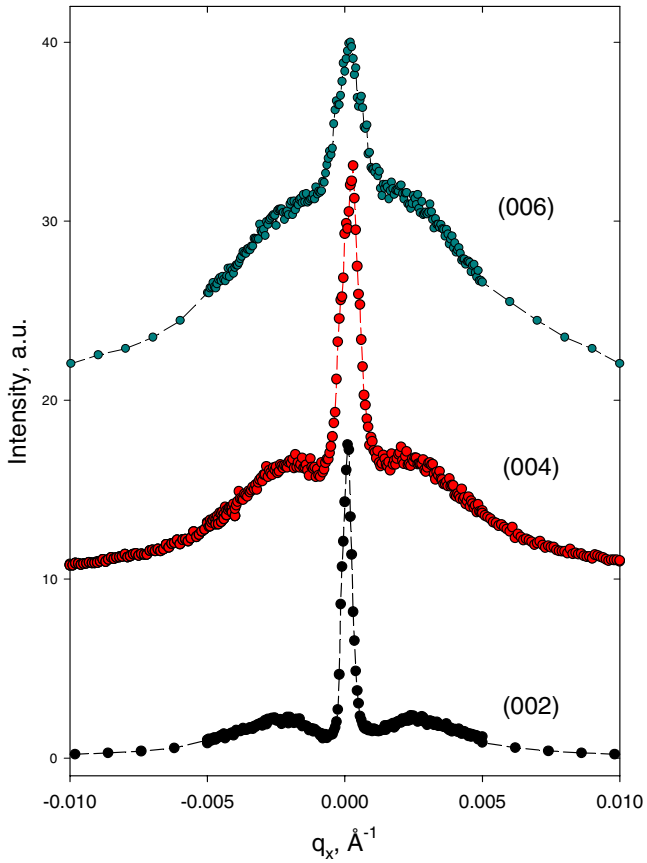

Figure 14. X-ray scattering from the (002), (004) and (006) reflections of a 123 Å thick GaSb layer measured in transverse scans parallel to the [1$\bar{1}$0] direction.

Table 3. 60° dislocation density ρ and dislocation spacing D in thick layers of GaSb.

Thickness (Å)	[110]		[1$\bar{1}$0]	
	ρ (Å^{-1})	D (Å)	ρ (Å^{-1})	D (Å)
1110	3.5×10^{-4}	2886	1.1×10^{-4}	9355
1590	6.6×10^{-4}	1505	1.6×10^{-4}	6170
2220	8.3×10^{-4}	1200	2.4×10^{-4}	4135
2845	1.9×10^{-3}	527	3.9×10^{-4}	2575

layers increases. The results are qualitatively consistent with previous electron microscopy and AFM measurements for GaSb layers grown on GaAs(001) substrates in that the large lattice mismatch is largely relaxed by 90° misfit dislocations arranged with a regular periodicity. This is consistent with the understanding of dislocation formation in a variety of heteroepitaxial systems and with previous results on the growth and relaxation of GaSb epilayers [2, 3, 5–9, 12, 14, 27]. The dislocations are generally of the 60° type when the misfit strain is small (<2%), are of mixed 60° and 90° types for intermediate degrees of misfit and are predominantly of the Lomer 90° type for very large degrees of misfit (>6%) [10]. Nevertheless, the type of

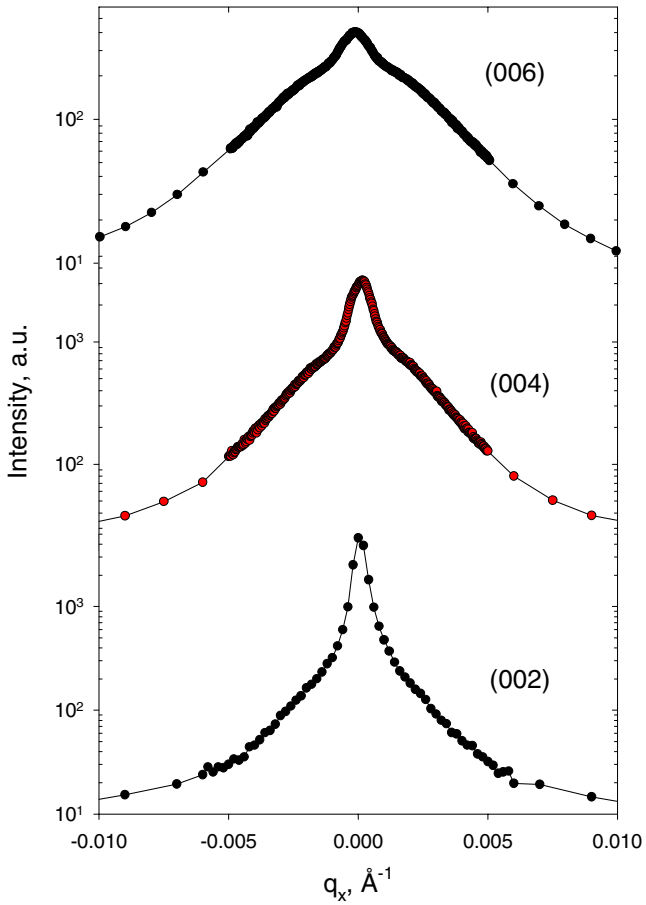

Figure 15. X-ray scattering from the (002), (004) and (006) reflections of a 220 Å thick GaSb layer measured in transverse scans parallel to the [110] direction.

dislocation depends also on the growth conditions. For example, when GaSb layers are grown on GaAs(001) at 520 °C the lattice mismatch strain is accommodated mainly by 90° dislocations but when grown at 540°C the misfit strain is relieved by both 90° and 60° dislocations and when grown at 560 °C the strain is accommodated mainly by 60° dislocations which cause a local tilt of the GaSb islands with respect to the GaAs substrate [6]. Our layers were grown at 520 °C and so have mostly 90° dislocations.

Our measurements show, however, that x-ray scattering can provide unique quantitative information about many aspects of the detailed structure. Initially we discussed the determination of the thicknesses of the layers and our best estimates of the thicknesses are listed in table 1. The results also clearly showed that there was a change in many of the properties for layers with a thickness of about 450 Å. The growth rate of the layers decreased for thicker layers, Pendellösung fringes were observed only for layers thinner than 450 Å, and the line-shape of longitudinal scans through the Bragg reflections changed from Gaussian for the thinner layers to a convolution of Gaussian and Lorentzian for the thicker layers. These results can be correlated with AFM measurements that show that up to thicknesses of approximately 300 Å the GaSb film is discontinuous and consists of islands [15]. When the

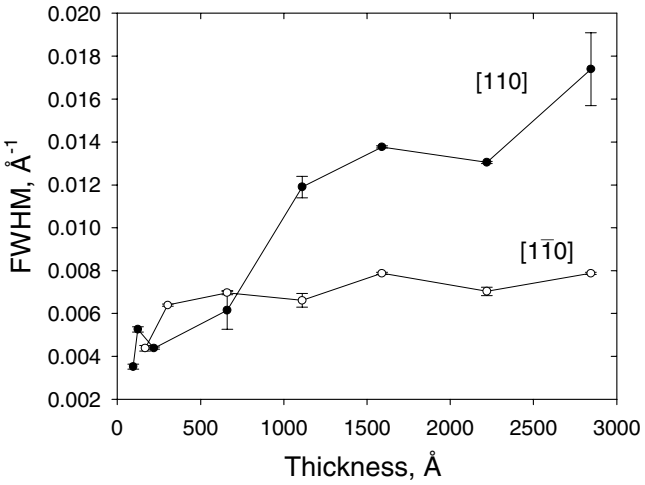

Figure 16. Width of the broad component of the diffuse scattering versus thickness for both the [1$\bar{1}$0] and [110] directions.

thickness increases, the size of the islands increases and individual islands begin to coalesce. When the thickness reaches 400 Å the individual islands can no longer be distinguished and the GaSb film covers the whole surface of the substrate and the growth mechanism changes from 3D to 2D. The AFM data show that the islands in thin (<200–300 Å) layers are much smaller than 10^4 Å. For example, the results shown in figure 1 show that the islands are anisotropic and are on average about 3000 Å long in the [110] direction and about 800 Å long in the [1$\bar{1}$0] direction while the spacing of the centres of the islands is about 6500 and 2000 Å respectively.

The x-ray scattering measurements show that most of the misfit strain is relieved by a regular array of 90° misfit dislocations and we have made a detailed study of the Bragg reflections from this dislocation lattice. The results are summarized in table 2 and show that the structure of the GaSb layers is orthorhombic with a periodic modulation due to the two intersecting arrays of 90° dislocations. The dislocations are located at the interface and both the layer and substrate (a GaAs buffer layer) are distorted. The coherence length of the distorted region in the growth direction does not change with the thickness whereas the density of dislocations does change. This result suggests that most of the crystal but a very narrow area near the interface is free from the 90° dislocations and almost free from the 60° dislocations up to approximately 1000 Å. When this thickness is reached the network of 60° dislocations gives the layer a mosaic structure.

The average spacing between the dislocations has been determined in both the [110] and [1$\bar{1}$0] directions and both decrease as the layer thickness increases. Since the dislocations are located at the interface it is surprising that their spacing changes when the thickness of the layers increases. The spacing of the dislocations, the relaxation and the residual in-plane strain are different along the [110] and [1$\bar{1}$0] directions, as detailed in figures 4 and 9 and in table 2. The strain is most fully relieved in the [1$\bar{1}$0] direction for which the islands have the smallest dimension. The correlation lengths for the dislocation lattice are typically 1400 Å for the [1$\bar{1}$0] direction, comparable to the spacing of the islands, and only about 800 Å for the [110] direction, which is considerably less than the island size. A large asymmetry in the relaxation, residual in-plane strains and a large ratio (up to 1.2–1.8) in the densities of misfit dislocations for the [110] and [1$\bar{1}$0] directions has been observed in other systems, for example

InGaAs/GaAs(001) [28–30], SiGe/Si(001) [21], $In_{1-x}Ga_xP$ and $GaAs_{1-x}P_x$ [18], which are mostly relaxed by 60°-type misfit dislocations. Their asymmetry is because the 60° dislocations of the same sign are preferentially being nucleated along the $[1\bar{1}0]$ direction [18, 21]. An asymmetry is also expected when the dislocations are 90° dislocations [17]. The difference in the dislocation density is then because of the different structure of the [110] and $[1\bar{1}0]$ dislocations: the two orthogonal dislocations cannot be coplanar as they lie on adjacent (001) planes[17]. The [110] 90° dislocations have a missing Ga atom in between two incompletely bonded Sb atoms and vice versa for the $[1\bar{1}0]$ dislocation. This difference in the bonding means that the dislocations have different energies leading to an asymmetry in the density of the dislocations. Since the dislocation spacing is larger for the dislocation array in the [110] direction, it is reasonable to expect that the energy of these dislocations will be larger.

Other aspects of the structure can be deduced from the scattering near to the Bragg reflections of bulk GaSb. For the thinner layers this scattering is characteristic of the scattering from islands. It consists of a Bragg-like sharp component and of a diffuse component. The former shows that the atomic planes are coherent over distance in excess of 10^4 Å, larger than the size of the islands. The atomic planes are therefore coherent on average between the different islands. The diffuse scattering arises from two contributions. One is due to a correlated distribution of the islands and the other from the displacements of the atoms from the ideal lattice positions. If only the former are present, the scattering is the same around each $00L$ reciprocal lattice point whereas if the displacements are small they give rise to scattering proportional to L^2. The wavevector dependence of the scattering, figure 14, shows that both components are present together, presumably with the corresponding interference effects.

In more detail the results obtained when the wavevector transfer was scanned in the $[1\bar{1}0]$ direction, figure 14, show peaks in the diffuse scattering at a wavevector that is independent of L. This is characteristic of the scattering from islands and the wavevector gives a measure, 2300 Å, of the spacing between the islands that is qualitatively consistent with the results of the AFM measurements. When the wavevector transfer is scanned along the [110] direction only a single peak is observed but this is possibly because it is not possible to separate the broad diffuse peaks from the Bragg-like peak as the distance between the islands is about three times larger. We have not so far developed a detailed model of the islands that is consistent with our x-ray scattering measurements but plan to develop the necessary techniques in the near future.

It is worth noting that the diffuse scattering from islands can be distinguished from that arising from 60° dislocations as we observed when GaSb layers were grown on InAs(001) [16]. The broad diffuse peaks from the islands have positions in wavevectors that are independent of L whereas the diffuse peaks from the dislocations have wavevectors that are roughly proportional to L.

The scattering from the thick layers ($T > 1200$ Å) is characteristic of a mosaic crystal with an asymmetric mosaic spread of 0.19° in the [110] direction and 0.11° in the $[1\bar{1}0]$ direction. The scattering profile is characteristic of a random network of dislocations [26] and the widths give the dislocation densities that are consistent with the numbers of dislocations needed to understand the difference between the relaxation of the whole structure and the relaxation due to the 90° dislocations shown in figure 9.

In conclusion we have made a detailed study of the structure of thin layers of GaSb grown on GaAs(001). This study illustrates the power of high-resolution x-ray scattering techniques for the non-destructive quantitative study of the structure of lattice mismatched materials. It provides a detailed description of the structure of the layers and of the dislocation networks. These results together with our earlier study of GaSb layers on InAs(001) show that x-ray scattering is a very sensitive tool to study thin layers whatever the lattice mismatch and to provide detailed information about the type and nature of the misfit dislocation networks.

Acknowledgments

The work was funded by the UK Engineering and Physical Sciences Research Council (EPSRC). Most of the experiments were performed on the EPSRC-funded XMaS (BM28) beam-line at the ESRF. We are grateful to the beam-line team for their invaluable assistance.

References

[1] Zheng L, Haywood S K, Mason N J and Verschoor G 2000 *IEE Proc.-Optoelectron.* **147** 205
[2] Aindow M, Cheng T T, Mason N J, Seong T-Y and Walker P J 1993 *J. Cryst. Growth.* **133** 168
[3] Rocher A *et al* 1991 *Inst. Phys. Conf. Ser. No. 117* (Bristol: Institute of Physics) pp 509–14 section 7
[4] Qian W, Skowronski M and Kaspi R 1997 *J. Electrochem. Soc.* **144** 1430
[5] Kang J M, Nouaoura M, Lassabatere L and Rocher A 1994 *J. Cryst. Growth* **143** 115
[6] Kim J-H, Seong T-Y, Mason N J and Walker P J 1998 *J. Electron. Mater.* **27** 466
[7] Rocher A and Kang J M 1995 *Inst. Phys. Conf. Ser. No. 146* (Bristol: Institute of Physics) pp 135–42
[8] Qian W, Skowronski M, Kaspi R, Graef M D and Dravid V P 1997 *J. Appl. Phys.* **81** 7268
[9] Rocher A M 1991 *Solid State Phenomena* vol 19/20 (Vaduz: Sci-Tech.) pp 563–72
[10] Mallard R E, Wilshaw P R, Mason N J, Walker P J and Booker G R 1989 *Inst. Phys. Conf. Ser. No. 100* (Bristol: Institute of Physics) pp 331–6 section 4
[11] Kang J M and Rocher A 1994 *Phil. Mag. Lett.* **70** 363
[12] Rocher A and Snoeck E 1998 *Thin Solid Films* **319** 172
[13] Rocher A M 1997 *Inst. Phys. Conf. Ser. No. 157* (Bristol: Institute of Physics) pp 153–6
[14] Bourret A and Fuoss P H 1992 *Appl. Phys. Lett.* **61** 1034
[15] Babkevich A, Cowley R A, Mason N J and Stunault A 2000 *J. Phys.: Condens. Matter* **12** 4747
[16] Babkevich A, Cowley R A, Mason N J, Sandiford S and Stunault A 2002 *J. Phys.: Condens. Matter* **14** 7101
[17] Abrahams M S and Buiocchi C J 1966 *J. Appl. Phys.* **37** 1973
[18] Abrahams M S, Blanc J and Buiocchi C J 1972 *Appl. Phys. Lett.* **21** 185
[19] Haasen P 1957 *Acta Met.* **5** 598
[20] Peissker E, Haasen P and Alexander H 1962 *Phil. Mag.* **7** 1279
[21] Stiffler S R, Stanis C L, Goorsky M, Chan K K and de Fresart E 1992 *J. Appl. Phys.* **71** 4820
[22] Booker G R *et al* 1997 *J. Cryst. Growth* **170** 777
[23] Bowen D and Wormington M 1993 *Adv. X-Ray Anal.* **36** 171
[24] Langford J I 1978 *J. Appl. Crystallogr.* **11** 10
[25] Langford J I 1992 *National Institute of Standards and Technology Special Publication* 846 (Location: National Institute of Standards and Technology) pp 110–25
[26] Kaganer V M, Köhler R, Schmidbauer M, Opitz R and Jenichen B 1997 *Phys. Rev.* B **55** 1793
[27] Beanland R, Dunstan D J and Goodhew P J 1996 *Europhys. J.* **45** 87
[28] Kavanagh K L, Chang J C P, Chen J, Fernandez J M and Wieder H H 1992 *J. Vac. Sci. Technol.* B **10** 1820
[29] Kavanagh K L *et al* 1988 *J. Appl. Phys.* **64** 4843
[30] Lazzarini L *et al* 1997 *Inst. Phys. Conf. Ser. No. 157* (Bristol: Institute of Physics) pp 149–52